

# BUCKLING AND POSTBUCKLING OF AXIALLY-LOADED CNT-REINFORCED COMPOSITE CYLINDRICAL SHELL SURROUNDED BY AN ELASTIC MEDIUM IN THERMAL ENVIRONMENT

Hoang Van Tung<sup>1,\*</sup>, Pham Thanh Hieu<sup>2</sup>

<sup>1</sup>Hanoi Architectural University, Vietnam

<sup>2</sup>University of Transport Technology, Hanoi, Vietnam

\*E-mail: [hoangtung0105@gmail.com](mailto:hoangtung0105@gmail.com)

Received: 31 May 2018 / Published online: 09 October 2018

**Abstract.** Buckling and postbuckling behaviors of nanocomposite cylindrical shells reinforced by single walled carbon nanotubes (SWCNTs), surrounded by an elastic medium, exposed to a thermal environment and subjected to uniform axial compression are investigated in this paper. Material properties of carbon nanotubes (CNTs) and isotropic matrix are assumed to be temperature dependent, and effective properties of nanocomposite are estimated by extended rule of mixture. The CNTs are embedded into matrix via uniform distribution (UD) or functionally graded (FG) distribution along the thickness direction. Governing equations are based on Donnell classical shell theory taking into account von Karman-Donnell nonlinear terms and interaction between the shell and surrounding elastic medium. Three-term form of deflection and stress function are assumed to satisfy simply supported boundary conditions and Galerkin method is applied to obtain load-deflection relation from which buckling and postbuckling behaviors are analyzed. Numerical examples are carried out to analyze the effects of CNT volume fraction and distribution types, geometrical ratios, environment temperature and surrounding elastic foundation on the buckling loads and postbuckling strength of nanocomposite cylindrical shells.

*Keywords:* CNT-reinforced composite; nanocomposite cylindrical shell; nonlinear stability; axial compression; elastic foundation.

## 1. INTRODUCTION

Carbon nanotubes (CNTs) have attracted huge attention in most areas of science and engineering due to their exceptional physical and mechanical properties. Single walled carbon nanotube (SWCNT) is a cylinder with diameter of order of 1 nm and length of up to centimeters and formed by seamless rolling a single sheet of graphene. No previous material has displayed extraordinary mechanical, thermal and electrical properties as CNTs. For example, the elastic modulus of SWCNT is approximately 1 TPa, the strength

of SWCNT up to 3.5 GPa, i.e. much higher than that of high-strength steel (2 GPa), and SWCNT has stability at tremendously high temperature up to 2800°C in vacuum and 750°C in air, etc [1,2]. In addition to these excellent characteristics, very high aspect ratio makes CNTs ideal as advanced reinforcing fillers into composites. Carbon nanotube reinforced composite (CNTRC) is a brilliant nanocomposite having numerous applications in most engineering areas and industries [3,4]. The CNT and CNTRC also have potential roles and expected applications for future generation of aircraft and space vehicles [5].

Motivated by concept of functionally graded material, Shen [6] first proposed functionally graded carbon nanotube reinforced composite (FG-CNTRC) properties of which are varied along the thickness direction according to functional rules to aim optimal distribution of CNTs and obtain desired response of nanocomposite structures. Stimulated by Shen's proposal, subsequent works relating to static and dynamic responses of FG-CNTRC plates and shells have been performed. Bending behavior of FG-CNTRC plates have been addressed in works [7,8] based on numerical methods and [9,10] using analytical methods. Linear buckling response of FG-CNTRC plates has been investigated in works [9] and [11] making use of analytical and semi-analytical solutions, respectively. Liew and co-workers [12,13] analyzed linear buckling of FG-CNTRC rectangular and skew plates under compressive loads by using mesh-free methods. Postbuckling problem of FG-CNTRC plates under thermal loads has been treated by Shen and Zhang [14] basing on a two-step perturbation technique, Kiani [15] utilizing Ritz method and Tung [16] using Galerkin method. Mechanical postbuckling of FG-CNTRC plates on elastic foundations under compression has been studied by Zhang and Liew [17] using an element-free approach.

Buckling and postbuckling behaviors of composite cylindrical panels reinforced by CNTs have been mentioned in some works. Nasihatgozar et al. [18] employed analytical solutions to analyze linear buckling of FG-CNTRC cylindrical panels with piezoelectric layers under axial compression. Linear buckling behavior of FG-CNTRC cylindrical panels under axial compression and shear loads has been examined by Macias et al. [19] basing on numerical simulation with shell finite elements. Nonlinear stability problem of axially compressed FG-CNTRC cylindrical panels has been dealt with by Shen and Xiang [20] employing a semi-analytical method and Liew et al. [21] using a meshless method. Shen and Xiang [22] and Shen [23] presented studies on postbuckling of FG-CNTRC cylindrical panels subjected to thermal load and external pressure, respectively. Recently, Trang and Tung [24,25] considered the effects of tangential restraints of boundary edges on the nonlinear stability of FG-CNTRC cylindrical panels under axial compression and external pressure in thermal environments.

Stability problem of closed shells such as FG-CNTRC circular cylindrical and conical shells has been addressed in some works. Based on a higher order shear deformation theory and a singular perturbation technique, buckling and postbuckling behaviors of FG-CNTRC cylindrical shells subjected to axial compression, external pressure and combined load have been investigated by Shen [26,27] and Shen and Xiang [28], respectively. By using a similar approach, Shen [29,30] conducted results of postbuckling analysis for FG-CNTRC cylindrical shells subjected to torsional and thermal loadings, respectively.

Based on Ritz energy approach, Ansari et al. [31] presented an analytical study on post-buckling behavior of FG-CNTRC cylindrical shells under axial compression and pressure loads. Ninh [32] used Galerkin method to investigate the postbuckling of FG-CNTRC cylindrical shells under torsional loading in thermal environment. Three-term solution of deflection and piezoelectric layers are taken into consideration in these works [31,32]. Linear buckling of FG-CNTRC conical shells under external pressure and thermal loading has been considered in works of Kiani and collaborators [33,34] making use of a semi-analytical approach. Mehri et al. [35] utilized harmonic differential quadrature method to solve buckling and vibration problems of FG-CNTRC truncated conical shells subjected to external pressure and axial compression simultaneously. Basing on a numerical approach with generalized differential quadrature method, Ansari and Torabi [36] studied the buckling and vibration of FG-CNTRC conical shells under axial compression.

Cylindrical shells are widely used in practical applications and appearance of carbon nanotubes augmented the potential applications of nanocomposite structures, especially nanocomposite cylindrical shells reinforced single-walled carbon nanotubes. Specifically, nanocomposite cylindrical shells are used in energy storage, mechanical systems and pressure pipes. Furthermore, nanocomposite cylindrical shells are expected to have potential applications in aerospace engineering [5]. The present study aims to investigate the buckling and postbuckling behaviors of cylindrical shells reinforced by single walled carbon nanotube (SWCNT), exposed to a thermal environment, surrounded by an elastic medium and mechanically loaded by uniform axial compression. Material properties are assumed to be temperature dependent, and effective properties of CNTRC are estimated through a micromechanical model based on the extended rule of mixture. CNTs are embedded into matrix phase through uniform distribution (UD) or functionally graded (FG) distribution. Basic equations are based on the classical shell theory incorporating von Karman-Donnell nonlinearity and foundation interaction according to Pasternak model. Three-term solution of deflection is assumed to satisfy simply supported boundary conditions and Galerkin method is applied to obtain nonlinear load-deflection relation from which buckling loads and postbuckling load-deflection curves are determined. Numerical examples are carried out to examine the effects of CNT volume fraction and distribution types, thermal environments, geometrical parameters and surrounding elastic medium on the nonlinear stability of axially loaded CNTRC cylindrical shells. The novelty of the present study results from an analytical approach with three-term solution of deflection and taking into account shell-surrounding elastic foundation interaction in analysis.

## 2. CNT-REINFORCED COMPOSITE CYLINDRICAL SHELL SURROUNDED BY AN ELASTIC MEDIUM

Consider a nanocomposite cylindrical shell reinforced by SWCNTs, surrounded by an elastic medium modelled as a two-parameter elastic foundation and defined in a coordinate system  $xyz$  origin of which is located on the middle surface at an end,  $x$  and  $y$  are in axial and circumferential directions, respectively, and  $z$  is perpendicular to the middle surface as shown in Fig. 1. The length, radius and thickness of the cylindrical shell are denoted by  $L$ ,  $R$  and  $h$ , respectively.

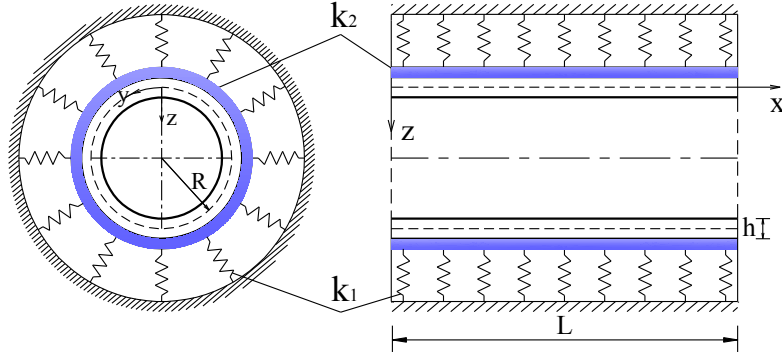


Fig. 1. Configuration and coordinate system of a cylindrical shell surrounded by an elastic medium

In this study, SWCNTs are reinforced into isotropic polymer matrix by uniform distribution (UD) or four functionally graded (FG) distributions named as FG-V, FG- $\Lambda$ , FG-O and FG-X types and extended rule of mixture is applied to determine effective Young moduli and shear modulus of the CNTRC shell as [6]

$$\begin{aligned}
 E_{11} &= \eta_1 V_{CNT} E_{11}^{CNT} + V_m E^m, \\
 \frac{\eta_2}{E_{22}} &= \frac{V_{CNT}}{E_{22}^{CNT}} + \frac{V_m}{E^m}, \\
 \frac{\eta_3}{G_{12}} &= \frac{V_{CNT}}{G_{12}^{CNT}} + \frac{V_m}{G^m},
 \end{aligned} \tag{1}$$

where  $E_{11}^{CNT}$ ,  $E_{22}^{CNT}$  and  $G_{12}^{CNT}$  are the Young moduli and shear modulus, respectively, of the CNT, whereas  $E^m$  and  $G^m$  are Young and shear moduli, respectively, of the isotropic matrix. Coefficients  $\eta_j$  ( $j = 1, 2, 3$ ), called the CNT efficiency parameters, are introduced into Eqs. (1) to consider the size-dependent material properties, whereas  $V_{CNT}$  and  $V_m$  are the volume fractions of CNTs and matrix, respectively, and their relation is  $V_{CNT} + V_m = 1$ .

The volume fraction  $V_{CNT}$  for five types of CNT distribution is assumed as

$$V_{CNT} = \begin{cases} V_{CNT}^* & \text{(UD)} \\ \left(1 + \frac{2z}{h}\right) V_{CNT}^* & \text{(FG-}\Lambda\text{)} \\ \left(1 - \frac{2z}{h}\right) V_{CNT}^* & \text{(FG-V)} \\ 2 \left(1 - \frac{2|z|}{h}\right) V_{CNT}^* & \text{(FG-O)} \\ 2 \left(\frac{2|z|}{h}\right) V_{CNT}^* & \text{(FG-X)} \end{cases} \tag{2}$$

where

$$V_{CNT}^* = \frac{w_{CNT}}{w_{CNT} + (\rho_{CNT}/\rho_m)(1 - w_{CNT})}, \quad (3)$$

in which  $w_{CNT}$  is the mass fraction of CNTs in the CNTRC shell,  $\rho_{CNT}$  and  $\rho_m$  are the densities of the CNTs and matrix, respectively. Poisson ratio depending weakly on position and temperature can be determined by

$$\nu_{12} = V_{CNT}^* \nu_{12}^{CNT} + V_m \nu^m, \quad (4)$$

where  $\nu_{12}^{CNT}$  and  $\nu^m$  are Poisson ratios of the CNT and matrix, respectively. The coefficients of thermal expansion of the CNTRC in the longitudinal and transverse directions have the form as [6, 14]

$$\begin{aligned} \alpha_{11} &= V_{CNT} \alpha_{11}^{CNT} + V_m \alpha^m, \\ \alpha_{22} &= (1 + \nu_{12}^{CNT}) V_{CNT} \alpha_{22}^{CNT} + (1 + \nu^m) V_m \alpha^m - \nu_{12} \alpha_{11}, \end{aligned} \quad (5)$$

where  $\alpha_{11}^{CNT}$ ,  $\alpha_{22}^{CNT}$  and  $\alpha^m$  are thermal expansion coefficients, respectively, of the CNT and isotropic matrix and, evidently,  $\alpha_{11}$  and  $\alpha_{22}$  are also graded in the thickness direction.

### 3. FORMULATIONS

Based on the classical shell theory (CST), strain components are expressed as

$$\varepsilon_x = \varepsilon_{x0} + z\chi_x, \quad \varepsilon_y = \varepsilon_{y0} + z\chi_y, \quad \gamma_{xy} = \gamma_{xy0} + 2z\chi_{xy}, \quad (6)$$

where strains of middle surface  $\varepsilon_{x0}$ ,  $\varepsilon_{y0}$ ,  $\gamma_{xy0}$  and curvature changes  $\chi_x$ ,  $\chi_y$ ,  $\chi_{xy}$  are related to displacements of middle surface  $u$ ,  $v$ ,  $w$  in coordinate directions  $x$ ,  $y$ ,  $z$ , respectively, as follows

$$\begin{pmatrix} \varepsilon_{x0} \\ \varepsilon_{y0} \\ \gamma_{xy0} \end{pmatrix} = \begin{pmatrix} u_{,x} + w_{,x}^2/2 \\ v_{,y} - w/R + w_{,y}^2/2 \\ u_{,y} + v_{,x} + w_{,x}w_{,y} \end{pmatrix}, \quad \begin{pmatrix} \chi_x \\ \chi_y \\ \chi_{xy} \end{pmatrix} = \begin{pmatrix} -w_{,xx} \\ -w_{,yy} \\ -w_{,xy} \end{pmatrix}, \quad (7)$$

where subscript prime indicates partial derivative and von Karman-Donnell nonlinear terms are retained.

Next, stress-strain relations of CNTRC shell are expressed as

$$\begin{pmatrix} \sigma_x \\ \sigma_y \\ \sigma_{xy} \end{pmatrix} = \begin{pmatrix} Q_{11} & Q_{12} & 0 \\ Q_{12} & Q_{22} & 0 \\ 0 & 0 & Q_{66} \end{pmatrix} \left( \begin{pmatrix} \varepsilon_x \\ \varepsilon_y \\ \gamma_{xy} \end{pmatrix} - \begin{pmatrix} \alpha_{11} \\ \alpha_{22} \\ 0 \end{pmatrix} \Delta T \right), \quad (8)$$

where

$$Q_{11} = \frac{E_{11}}{1 - \nu_{12}\nu_{21}}, \quad Q_{22} = \frac{E_{22}}{1 - \nu_{12}\nu_{21}}, \quad Q_{66} = G_{12}, \quad (9)$$

and  $\Delta T$  is uniform temperature rise from thermal stress free initial state.

Based on the CST, force and moment resultants are expressed as

$$\begin{aligned} (N_x, M_x) &= (e_{11}, e_{12}) \varepsilon_{x0} + \nu_{21} (e_{11}, e_{12}) \varepsilon_{y0} + (e_{12}, e_{13}) \chi_x + \nu_{21} (e_{12}, e_{13}) \chi_y - (e_{11T}, e_{12T}) \Delta T, \\ (N_y, M_y) &= \nu_{12} (e_{21}, e_{22}) \varepsilon_{x0} + (e_{21}, e_{22}) \varepsilon_{y0} + \nu_{12} (e_{22}, e_{23}) \chi_x + (e_{22}, e_{23}) \chi_y - (e_{21T}, e_{22T}) \Delta T, \\ (N_{xy}, M_{xy}) &= (e_{31}, e_{32}) \gamma_{xy0} + 2 (e_{32}, e_{33}) \chi_{xy}, \end{aligned} \quad (10)$$

where

$$\begin{aligned} (e_{11}, e_{12}, e_{13}) &= \int_{-h/2}^{h/2} Q_{11} (1, z, z^2) dz, \\ (e_{21}, e_{22}, e_{23}) &= \int_{-h/2}^{h/2} Q_{22} (1, z, z^2) dz, \quad (e_{31}, e_{32}, e_{33}) = \int_{-h/2}^{h/2} Q_{66} (1, z, z^2) dz, \\ (e_{11T}, e_{12T}) &= \int_{-h/2}^{h/2} Q_{11} (\alpha_{11} + \nu_{21} \alpha_{22}) (1, z) dz, \quad (e_{21T}, e_{22T}) = \int_{-h/2}^{h/2} Q_{22} (\nu_{12} \alpha_{11} + \alpha_{22}) (1, z) dz. \end{aligned} \quad (11)$$

Based on the CST, nonlinear equilibrium equations for a cylindrical shell surrounded by an elastic medium are

$$\begin{aligned} N_{x,x} + N_{xy,y} &= 0, \\ N_{xy,x} + N_{y,y} &= 0, \\ M_{x,xx} + 2M_{xy,xy} + M_{y,yy} + N_x w_{,xx} + 2N_{xy} w_{,xy} + N_y w_{,yy} + N_y/R - q_f &= 0, \end{aligned} \quad (12)$$

where  $q_f$  is interactive pressure resulting from surrounding elastic medium and represented by Pasternak model as

$$q_f = k_1 w - k_2 \Delta w, \quad (13)$$

in which  $k_1$  is Winkler foundation modulus,  $k_2$  is stiffness of shear layer in Pasternak model and  $\Delta = \partial^2/\partial x^2 + \partial^2/\partial y^2$  is Laplace operator.

From Eqs. (7) and (10), equilibrium equation of CNTRC cylindrical shell is rewritten in the form as

$$\begin{aligned} a_{11} w_{,xxxx} + a_{21} w_{,yyyy} + a_{31} w_{,xxyy} + a_{41} f_{,xxyy} - f_{,yy} w_{,xx} + 2f_{,xy} w_{,xy} \\ - f_{,xx} w_{,yy} - \frac{f_{,xx}}{R} + k_1 w - k_2 (w_{,xx} + w_{,yy}) = 0, \end{aligned} \quad (14)$$

where  $f(x, y)$  is a stress function defined as

$$N_x = f_{,yy}, \quad N_y = f_{,xx}, \quad N_{xy} = -f_{,xy}, \quad (15)$$

and coefficients  $a_{11}$ ,  $a_{21}$ ,  $a_{31}$ ,  $a_{41}$  are given as in the work [16].

Subsequently, strain compatibility equation of a cylindrical shell has the form as

$$\varepsilon_{x0,yy} + \varepsilon_{y0,xx} - \gamma_{xy0,xy} = w_{,xy}^2 - w_{,xx} w_{,yy} - w_{,xx}/R. \quad (16)$$

By virtue of Eqs. (7), (10) and (15), the strain compatibility equation of a geometrically perfect CNTRC cylindrical shell is written in the form

$$a_{12}f_{,xxxx} + a_{22}f_{,xxyy} + a_{32}f_{,yyyy} + a_{42}w_{,xxxx} + a_{52}w_{,xxyy} + a_{62}w_{,yyyy} - w_{,xy}^2 + w_{,xx}w_{,yy} + \frac{w_{,xx}}{R} = 0, \quad (17)$$

where coefficients  $a_{i2}$  ( $i = 1 \div 6$ ) have been defined in the works [24, 25].

The present study considers simply supported CNTRC cylindrical shells with freely movable edges and the associated boundary conditions are expressed as

$$w = 0, \quad M_x = 0, \quad N_{xy} = 0, \quad N_x = N_{x0} \quad \text{at} \quad x = 0, L \quad (18)$$

where  $N_{x0} = -Ph$  is prebuckling force resultant in which  $P$  is axial pressure uniformly compressed on two boundary surfaces of cylindrical shell.

To satisfy approximately boundary conditions (18), the following solutions of deflection and stress function are assumed [31, 37–39]

$$w(x, y) = W_0 + W_1 \sin \beta_m x \sin \delta_n y + W_2 \sin^2 \beta_m x, \quad (19)$$

$$f(x, y) = A_1 \cos 2\beta_m x + A_2 \cos 2\delta_n y + A_3 \sin \beta_m x \sin \delta_n y + A_4 \sin 3\beta_m x \sin \delta_n y - \sigma_{0y} h \frac{x^2}{2} + N_{x0} \frac{y^2}{2}, \quad (20)$$

where  $\beta_m = m\pi/L$ ,  $\delta_n = n/R$  with  $m, n$  are numbers of half wave and full wave in axial and circumferential directions, respectively,  $W_0, W_1$  and  $W_2$  are unknown amplitudes corresponding to prebuckling, linear buckling and nonlinear buckling states of the deflection, respectively. In addition, in Eq. (20),  $\sigma_{0y}$  is average stress in circumferential direction and  $A_i$  ( $i = 1 \div 4$ ) are coefficients to be determined.

Next, introduction of solutions (19) and (20) into the compatibility equation (17) gives the following results

$$A_1 = \frac{1}{32a_{12}\beta_m^2} \left( \delta_n^2 W_1^2 + 16a_{42}\beta_m^2 W_2 - \frac{4}{R} W_2 \right), \quad A_2 = \frac{\beta_m^2 W_1^2}{32a_{32}\delta_n^2},$$

$$A_3 = \frac{W_1}{a_{12}\beta_m^4 + a_{22}\beta_m^2\delta_n^2 + a_{32}\delta_n^4} \left( \frac{\beta_m^2}{R} - a_{42}\beta_m^4 - a_{52}\beta_m^2\delta_n^2 - a_{62}\delta_n^4 - \beta_m^2\delta_n^2 W_2 \right), \quad (21)$$

$$A_4 = \frac{\beta_m^2\delta_n^2 W_1 W_2}{81a_{12}\beta_m^4 + 9a_{22}\beta_m^2\delta_n^2 + a_{32}\delta_n^4}.$$

Now, solutions (19) and (20) are substituted into equilibrium equation (14), then applying Galerkin method on whole region of the shell ( $0 \leq x \leq L, 0 \leq y \leq 2\pi R$ ) to the resulting equilibrium equation yields the following expressions

$$\sigma_{0y} \frac{h}{R} + k_1 \left( W_0 + \frac{W_2}{2} \right) = 0, \quad (22a)$$

$$a_{13} - a_{23}W_2 + a_{33}W_1^2 + a_{43}W_2^2 + N_{x0}\beta_m^2 - \sigma_{0y}h\delta_n^2 = 0, \quad (22b)$$

$$k_1 W_0 + a_{14}W_2 - a_{24}W_1^2 + a_{34}W_1^2 W_2 + \beta_m^2 N_{x0} W_2 + \sigma_{0y} \frac{h}{R} = 0, \quad (22c)$$

where coefficients  $a_{j3}$  ( $j = 1 \div 4$ ) and  $a_{k4}$  ( $k = 1 \div 3$ ) are displayed in Eq. (A1) of Appendix A.

For circular cylindrical shell, the following circumferential closed condition must be satisfied

$$\int_0^{2\pi R} \int_0^L \frac{\partial v}{\partial y} dx dy = \int_0^{2\pi R} \int_0^L \left( \varepsilon_{0y} + \frac{w}{R} - \frac{1}{2} w_{,y}^2 \right) dx dy = 0. \quad (23)$$

From Eqs. (7), (10) and (15),  $v_{,y}$  is expressed in terms of partial derivatives of  $w$  and  $f$ . Then placing the solutions (19), (20) into the  $v_{,y}$  and substitution of the obtained result into Eq. (23) yield the following relation

$$\begin{aligned} \sigma_{0y} h = & -\frac{\nu_{12} e_{21}}{e_{11}} N_{x0} + \left( e_{21T} - \nu_{12} \frac{e_{21}}{e_{11}} e_{11T} \right) \Delta T \\ & + (1 - \nu_{12} \nu_{21}) e_{21} \left[ \frac{1}{R} \left( W_0 + \frac{W_2}{2} \right) - \frac{\delta_n^2}{8} W_1^2 \right]. \end{aligned} \quad (24)$$

Introduction of  $N_{x0} = -Ph$  and  $\sigma_{0y} h$  from Eq. (24) into Eqs. (22) give the following system of equations

$$f_{11} (2\bar{W}_0 + \bar{W}_2) - f_{21} \bar{W}_1^2 + f_{31} P + f_{41} \Delta T = 0, \quad (25)$$

$$f_{12} - f_{22} \bar{W}_0 - f_{32} \bar{W}_2 + f_{42} \bar{W}_1^2 + f_{52} \bar{W}_2^2 - f_{62} P - f_{72} \Delta T = 0, \quad (26)$$

$$f_{13} \bar{W}_0 + f_{23} \bar{W}_2 - f_{33} \bar{W}_1^2 + f_{43} \bar{W}_1^2 \bar{W}_2 - (f_{53} \bar{W} - f_{63}) P + f_{73} \Delta T = 0, \quad (27)$$

where the details of coefficients  $f_{i1}$  ( $i = 1 \div 4$ ),  $f_{j2}$  ( $j = 1 \div 7$ ) and  $f_{k3}$  ( $k = 1 \div 7$ ) can be found in Eq. (A2) of Appendix A in which

$$(\bar{a}_{11}, \bar{a}_{21}, \bar{a}_{31}, \bar{e}_{13}, \bar{e}_{23}, \bar{e}_{33}) = \frac{1}{h^3} (a_{11}, a_{21}, a_{31}, e_{13}, e_{23}, e_{33}), \quad (\bar{a}_{12}, \bar{a}_{22}, \bar{a}_{32}) = (a_{12}, a_{22}, a_{32}) h,$$

$$(\bar{a}_{41}, \bar{a}_{42}, \bar{a}_{52}, \bar{a}_{62}, \bar{e}_{11}, \bar{e}_{21}, \bar{e}_{31}, \bar{W}_0, \bar{W}_1, \bar{W}_2) = \frac{1}{h} (a_{41}, a_{42}, a_{52}, a_{62}, e_{11}, e_{21}, e_{31}, W_0, W_1, W_2),$$

$$(\bar{e}_{12}, \bar{e}_{22}, \bar{e}_{32}) = \frac{1}{h^2} (e_{12}, e_{22}, e_{32}),$$

$$R_h = R/h, \quad L_R = L/R, \quad (K_1, K_2) = (k_1 R^2, k_2) \frac{R^2}{E_0^m h^3}, \quad (28)$$

with  $E_0^m$  is value of  $E^m$  calculated at room temperature ( $T_0 = 300$  K).

It is deduced from Eqs. (25) and (26) that

$$\begin{aligned} \bar{W}_0 &= f_{14} \bar{W}_2 + f_{24} \bar{W}_2^2 + f_{34} P + f_{44} \Delta T - f_{54}, \\ \bar{W}_1^2 &= f_{15} \bar{W}_2 + f_{25} \bar{W}_2^2 + f_{35} P + f_{45} \Delta T - f_{55}, \end{aligned} \quad (29)$$

where detailed definitions of coefficients  $f_{i4}, f_{i5}$  ( $i = 1 \div 5$ ) are given in Eq. (B1) of Appendix B.

Introduction of Eqs. (29) into Eq. (27) leads to the following relation

$$P = \frac{1}{f_{16} + f_{26} \bar{W}_2} [f_{36} + f_{46} \bar{W}_2 + f_{56} \bar{W}_2^2 + f_{66} \bar{W}_2^3 - (f_{76} + f_{86} \bar{W}_2) \Delta T], \quad (30)$$

where coefficients  $f_{j6}$  ( $j = 1 \div 8$ ) are displayed in Eq. (B3) of Appendix B.

From Eq. (30), by setting  $\bar{W}_2 = 0$ , buckling loads of axially-loaded CNTRC cylindrical shells  $P_b$  are obtained as

$$P_b = \frac{1}{f_{16}} (f_{36} - f_{76}\Delta T). \quad (31)$$

Critical buckling compression load  $P_{cr}$  is the smallest value among buckling loads  $P_b$  with respect to  $m$ ,  $n$  numbers representing buckling mode.

It is evident from Eq. (19) that maximum deflection of the cylindrical shell is

$$W_{\max} = W_0 + W_1 + W_2. \quad (32)$$

It is deduced from Eqs. (29) and (32) that non-dimensional maximum deflection of the CNTRC cylindrical shells are expressed as

$$\begin{aligned} \bar{W}_{\max} = W_{\max}/h = & (f_{14} + 1) \bar{W}_2 + f_{24} \bar{W}_2^2 + f_{34} P + f_{44} \Delta T - f_{54} \\ & + (f_{15} \bar{W}_2 + f_{25} \bar{W}_2^2 + f_{35} P + f_{45} \Delta T - f_{55})^{1/2}. \end{aligned} \quad (33)$$

The postbuckling equilibrium paths, i.e. axial compression load – non-dimensional maximum deflection curves, of the CNTRC cylindrical shells are traced from Eqs. (30) and (33).

#### 4. RESULTS AND DISCUSSION

This section presents numerical examples for buckling and postbuckling analysis of CNTRC cylindrical shell made of Poly (methyl methacrylate), referred to as PMMA, as matrix material and reinforced by (10,10) SWCNTs. The temperature dependent properties of the PMMA are  $E^m = (3.52 - 0.0034T)$  GPa,  $\alpha^m = 45 (1 + 0.0005\Delta T) \times 10^{-6} \text{ K}^{-1}$ ,  $\nu^m = 0.34$  in which  $T = T_0 + \Delta T$  and  $T_0 = 300 \text{ K}$  (room temperature). The temperature dependent properties of the (10,10) SWCNTs are given at discrete values of temperature in works [14,19,30] and as continuous functions of temperature in the work [23] and are omitted here for sake of brevity. The CNT efficiency parameters  $\eta_j$  ( $j = 1 \div 3$ ) are estimated by matching the Young moduli  $E_{11}$ ,  $E_{22}$  and shear modulus  $G_{12}$  of the CNTRC determined from the extended rule of mixture to those from the molecular dynamics (MD) simulations and given in the works [14,23,30,39,40] as  $(\eta_1, \eta_2, \eta_3) = (0.137, 1.022, 0.715)$  for case of  $V_{CNT}^* = 0.12$ ,  $(\eta_1, \eta_2, \eta_3) = (0.142, 1.626, 1.138)$  for case of  $V_{CNT}^* = 0.17$  and  $(\eta_1, \eta_2, \eta_3) = (0.141, 1.585, 1.109)$  for case of  $V_{CNT}^* = 0.28$ .

##### 4.1. Verification

To verify the proposed approach, the nonlinear buckling response of thin CNTRC cylindrical shells without surrounding elastic medium and subjected to uniform axial compression is considered. Critical buckling forces of thin CNTRC cylindrical shells with simply supported and movable boundary edges are given in Tab. 1 in comparison with results of Shen [26] using the higher order shear deformation shell theory and asymptotic solutions. Specifically, in the work [26], deflection, stress function and rotations are expressed in terms of regular and boundary layer solutions expanded into a small perturbation parameter. Then, with an initial buckling mode assumed, a singular perturbation technique is employed to determine the buckling loads and postbuckling equilibrium

paths. Although the method used in the work [26] has good accuracy, its mathematical cumbersomeness is considerable. It is evident that an excellent agreement is obtained in this comparison.

Table 1. Comparisons of critical buckling forces  $F_{cr} = 2\pi RhP_{cr}$  (in kN) of thin CNTRC cylindrical shells under axial compression [ $R/h = 100$ ,  $h = 1$  mm,  $T = 300$  K,  $(K_1, K_2) = (0, 0)$ ]

$L/R$	Source	$V_{CNT}^* = 0.12$		$V_{CNT}^* = 0.17$		$V_{CNT}^* = 0.28$	
		UD	FG-X	UD	FG-X	UD	FG-X
1	Shen [26]	18.75	21.81	30.43	35.53	37.77	47.18
	Present	18.84 <sup>a</sup>	21.76	30.54	35.44	38.02	47.40
$\sqrt{3}$	Shen [26]	19.35	22.06	31.11	37.06	39.60	46.52
	Present	19.48 <sup>b</sup>	22.01	31.28 <sup>b</sup>	36.99	39.95	46.81
$\sqrt{5}$	Shen [26]	18.72	21.37	30.57	35.14	37.31	45.99
	Present	18.78 <sup>c</sup>	21.30	30.66	35.04	37.49	46.21

<sup>a</sup> $(m, n) = (1, 7)$  for  $L/R = 1$ ; <sup>b</sup> $(m, n) = (2, 7)$ , otherwise  $(m, n) = (1, 6)$  for  $L/R = \sqrt{3}$ ;  
<sup>c</sup> $(m, n) = (2, 7)$  for  $L/R = \sqrt{5}$ .

In what follows, the buckling and postbuckling behaviors of CNTRC cylindrical shells will be analyzed in tabular and graphical forms, respectively. For sake of brief expression, CNTRC cylindrical shells are assumed to be without foundation interaction and placed at room temperature ( $T = 300$  K) unless otherwise specified.

#### 4.2. Buckling analysis

The effects of CNT volume fraction  $V_{CNT}^*$ , CNT distribution types and thermal environments ( $T = 300$  K,  $400$  K,  $500$  K) on the critical buckling loads of CNTRC cylindrical shells under axial compression are shown in Tab. 2. It is evident that FG-O and FG-X types of CNT distribution give the lowest and highest critical loads of CNTRC cylindrical shells, respectively. The critical loads of UD shells are slightly higher than those of the FG-V shells and, similarly, the critical loads of FG- $\Lambda$  shells are slightly higher than those of the FG-O shells. In addition, the critical buckling loads of CNTRC shells are considerably enhanced and difference between critical loads with different distribution types is bigger as CNT volume fraction is increased. Furthermore, the critical buckling compression loads of CNTRC shells are decreased when environment temperature is elevated.

Tab. 3 assesses the effects of geometrical ratios  $L/R$ ,  $R/h$  and elastic media on the critical buckling loads of CNTRC cylindrical shells under axial compression. There is no a definite trend of critical loads versus length-to-radius  $L/R$  ratio and, with different numbers of half wave  $m$ , critical loads of CNTRC cylindrical shells with  $L/R = 1$  and  $L/R = 2$  are the same. Otherwise, the critical buckling loads of CNTRC cylindrical shells are rapidly dropped when radius-to-thickness  $R/h$  ratio is increased. Moreover, surrounding elastic foundations have beneficial effects on the buckling resistance capability of CNTRC cylindrical shells.

Table 2. Effects of CNT volume fraction and distribution types on critical loads  $P_{cr}$  (in MPa) of CNTRC cylindrical shells [ $R/h = 100$ ,  $L/R = 1$ ,  $(m, n) = (1, 7)$ ,  $(K_1, K_2) = (0, 0)$ ]

$V_{CNT}^*$	$T$ (K)	UD	FG-X	FG-O	FG- $\Lambda$	FG-V
0.12	300	29.98	34.64	25.60	25.63	29.51
	400	26.88	31.38	22.63	22.80	26.17
	500	23.82	28.18	19.68	20.01	22.86
0.17	300	48.61	56.41	41.91	42.26	48.36
	400	43.46	50.88	36.99	37.50	42.80
	500	38.36	45.46	32.08	32.78	37.26
0.28	300	60.51	75.45	50.40	53.71	59.10
	400	54.59	68.63	44.75	47.97	52.65
	500	48.79	61.98	39.14	42.31	46.25

Table 3. Effects of geometrical ratios and elastic media on the critical buckling loads  $P_{cr}$  (in MPa) of FG-X CNTRC cylindrical shells under axial compression ( $V_{CNT}^* = 0.17$ ,  $T = 300$  K)

$L/R$	$(K_1, K_2)$	$R/h$			
		60	80	100	150
1	(0, 0)	104.95 (1, 6)	73.36 (1, 6)	56.41 (1, 7)	36.86 (1, 8)
	(100, 0)	111.92 (1, 6)	77.30 (1, 6)	58.92 (1, 7)	37.98 (1, 8)
	(100, 5)	126.57 (1, 5)	86.38 (1, 6)	66.38 (1, 7)	42.14 (1, 8)
1.5	(0, 0)	92.31 (1, 5)	70.28 (1, 6)	56.74 (1, 6)	38.66 (2, 9)
	(100, 0)	108.05 (1, 5)	79.13 (1, 6)	62.42 (1, 6)	39.28 (2, 9)
	(100, 5)	131.29 (1, 5)	94.63 (1, 5)	70.46 (2, 7)	42.17 (2, 8)
2	(0, 0)	104.95 (2, 6)	73.36 (2, 6)	56.41 (2, 7)	36.86 (2, 8)
	(100, 0)	111.92 (2, 6)	77.30 (2, 6)	58.92 (2, 7)	37.98 (2, 8)
	(100, 5)	126.57 (2, 5)	86.38 (2, 6)	66.38 (2, 7)	42.14 (2, 8)

It is noted that variation trend of critical buckling loads versus different values of  $V_{CNT}^*$ ,  $T$  and  $L/R$  is similar to that in the work [26] in which only UD and FG-X shells are considered.

### 4.3. Postbuckling analysis

In what follows, the postbuckling behavior of axially-loaded CNTRC cylindrical shells is graphically analyzed. Fig. 2 shows the effects of five different types of CNT distribution on the postbuckling of CNTRC cylindrical shells under axial compression. As can be seen, the FG-X and FG-O types give the strongest and weakest postbuckling strengths of CNTRC cylindrical shells, respectively. The FG-V shell has quite high load carrying capacity in small region of deflection (about  $W_{max}/h \leq 1$  in this example) but experience a relatively severe snap-through response. The UD shell has quite high and stable postbuckling equilibrium path, although buckling load and initial postbuckling

strength of this shell are lower than those of the FG-V shell. It is recognized that snap-through phenomenon, intensity of which is measured by difference between bifurcation point and the lowest point on load-deflection path, of CNTRC circular cylindrical shell is more severe than that of CNTRC cylindrical panels [24] under axial compression. Subsequently, the effects of CNT volume fraction  $V_{CNT}^*$  ( $= 0.12$  and  $0.17$ ) and thermal environments  $\Delta T$  ( $= 0$  and  $100$  K) on the postbuckling behavior of FG-X CNTRC cylindrical shells subjected to axial compression are analyzed in Fig. 3.

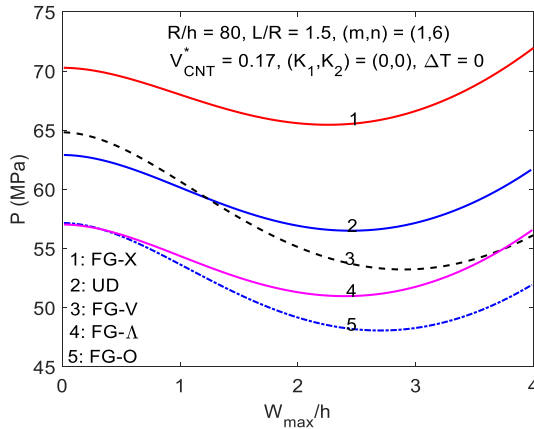


Fig. 2. Effects of CNT distribution types on the postbuckling behavior of CNTRC cylindrical shells under axial compression

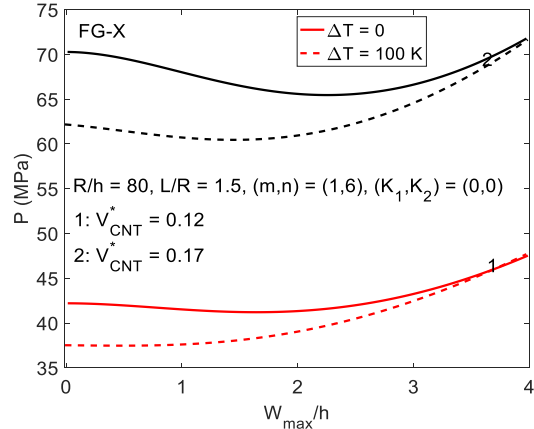


Fig. 3. Effects of CNT volume fraction and thermal environments on the postbuckling of FG-X CNTRC cylindrical shells

Obviously, load-deflection curves of CNTRC cylindrical shells are significantly increased as CNT volume fraction is increased. Under axial compression loading condition, volume percentage of CNT has sensitive effects on the buckling load and postbuckling load carrying capacity of CNTRC shells. In contrast, the postbuckling curves of axially-loaded CNTRC shells become lower, especially in small region of deflection, due to increase in environment temperature. Fig. 3 also indicates that intensity of snap-through response and detrimental influence of elevated temperature both become more severe at higher value of CNT volume percentage (i.e. CNT-richer shells).

Again, the simultaneous effects of CNT distribution and thermal environments on the postbuckling behavior of CNTRC cylindrical shells are considered in Fig. 4. It is realized that FG-V shell is more sensitive to change of environment temperature. Specifically, decrease in axial load-deflection curves due to high temperature is more pronounced for FG-V type of CNT distribution. Next, the effects of radius-to-thickness  $R/h$  ratio on the postbuckling behavior of FG-CNTRC cylindrical shells surrounded by Winkler elastic foundation and loaded by axial compression are examined in Fig. 5. It is clear that load-deflection equilibrium paths are rapidly reduced when  $R/h$  ratio is increased. Furthermore, number of full wave  $n$  in circumferential direction is increased as CNTRC cylindrical shell becomes thinner.

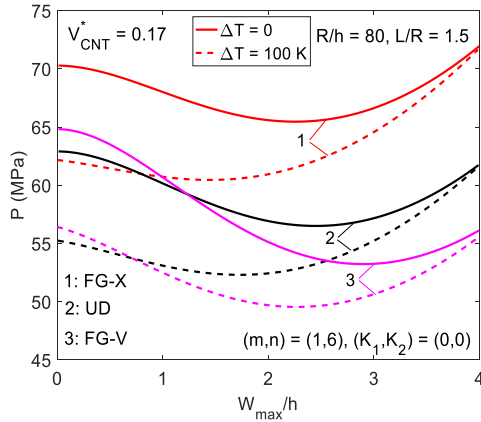


Fig. 4. Effects of CNT distribution and thermal environments on the postbuckling of CNTRC cylindrical shells

Finally, the effects of surrounding elastic foundations on the postbuckling behavior of FG-CNTRC cylindrical shells subjected to axial compression are given in Fig. 6. It is evident that surrounding elastic foundations have beneficial influences on the nonlinear stability of axially-loaded CNTRC cylindrical shells. More specifically, although severity of snap-through response is not milder, both buckling load and postbuckling equilibrium path are pronouncedly enhanced due to the embrace of elastic foundations, especially Pasternak type foundations.

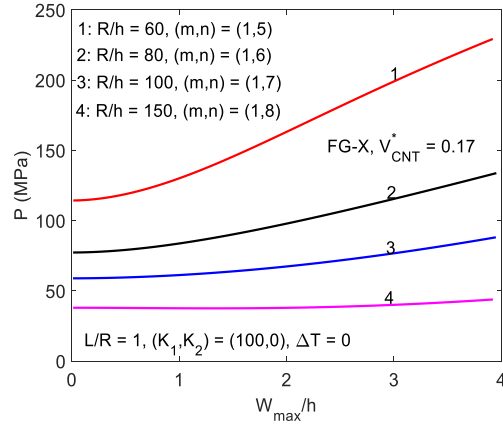


Fig. 5. Effects of radius-to-thickness ratio on the postbuckling of CNTRC cylindrical shell surrounded by Winkler foundation

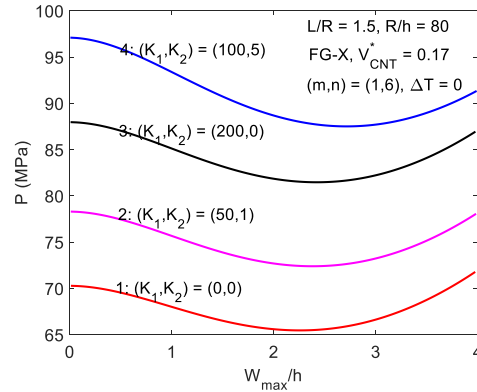


Fig. 6. Effects of surrounding elastic media on the postbuckling behavior of FG-CNTRC cylindrical shells under axial compression

## 5. CONCLUDING REMARKS

Based on an analytical approach with three-term solution of deflection and Galerkin method, nonlinear buckling and postbuckling behaviors of simply supported thin CNTRC circular cylindrical shells surrounded by elastic media and subjected to uniform axial compression have been presented. The results show that CNT volume fraction has very sensitive effects on the buckling load, postbuckling strength and snap-through response of CNTRC cylindrical shells. FG-X type shells have the best postbuckling behavior in general, and FG-V type shells have relatively high equilibrium paths in small region of postbuckling response in particular. The study also indicates that elevated temperature has deteriorative effects on buckling resistance and postbuckling load carrying capabilities of CNTRC cylindrical shells, and these effects are more pronounced in small

region of deflection. As a final remark, although intensity of snap-through instability is not reduced, surrounding elastic foundations, especially Pasternak type foundations, have significant and beneficial influences on buckling resistance and postbuckling response of axially-loaded CNTRC cylindrical shells.

### ACKNOWLEDGMENT

This research is funded by Vietnam National Foundation for Science and Technology Development (NAFOSTED) under grant number 107.02-2017.11.

### REFERENCES

- [1] J. N. Coleman, U. Khan, W. J. Blau, and Y. K. Gun'ko. Small but strong: a review of the mechanical properties of carbon nanotube–polymer composites. *Carbon*, **44**, (9), (2006), pp. 1624–1652. <https://doi.org/10.1016/j.carbon.2006.02.038>.
- [2] E. T. Thostenson, C. Li, and T. W. Chou. Nanocomposites in context. *Composites Science and Technology*, **65**, (3-4), (2005), pp. 491–516. <https://doi.org/10.1016/j.compscitech.2004.11.003>.
- [3] M. Paradise and T. Goswami. Carbon nanotubes–production and industrial applications. *Materials & Design*, **28**, (5), (2007), pp. 1477–1489. <https://doi.org/10.1016/j.matdes.2006.03.008>.
- [4] A. M. K. Esawi and M. M. Farag. Carbon nanotube reinforced composites: potential and current challenges. *Materials & Design*, **28**, (9), (2007), pp. 2394–2401. <https://doi.org/10.1016/j.matdes.2006.09.022>.
- [5] O. Gohardani, M. C. Elola, and C. Elizetxea. Potential and prospective implementation of carbon nanotubes on next generation aircraft and space vehicles: A review of current and expected applications in aerospace sciences. *Progress in Aerospace Sciences*, **70**, (2014), pp. 42–68. <https://doi.org/10.1016/j.paerosci.2014.05.002>.
- [6] H. S. Shen. Nonlinear bending of functionally graded carbon nanotube-reinforced composite plates in thermal environments. *Composite Structures*, **91**, (1), (2009), pp. 9–19. <https://doi.org/10.1016/j.compstruct.2009.04.026>.
- [7] P. Phung-Van, M. Abdel-Wahab, K. M. Liew, S. P. A. Bordas, and H. Nguyen-Xuan. Iso-geometric analysis of functionally graded carbon nanotube-reinforced composite plates using higher-order shear deformation theory. *Composite Structures*, **123**, (2015), pp. 137–149. <https://doi.org/10.1016/j.compstruct.2014.12.021>.
- [8] L. W. Zhang, Z. G. Song, and K. M. Liew. Nonlinear bending analysis of FG-CNT reinforced composite thick plates resting on Pasternak foundations using the element-free IMLS-Ritz method. *Composite Structures*, **128**, (2015), pp. 165–175. <https://doi.org/10.1016/j.compstruct.2015.03.011>.
- [9] N. Wattanasakulpong and A. Chaikittiratana. Exact solutions for static and dynamic analyses of carbon nanotube-reinforced composite plates with Pasternak elastic foundation. *Applied Mathematical Modelling*, **39**, (18), (2015), pp. 5459–5472. <https://doi.org/10.1016/j.apm.2014.12.058>.
- [10] A. Alibeigloo and K. M. Liew. Thermoelastic analysis of functionally graded carbon nanotube-reinforced composite plate using theory of elasticity. *Composite Structures*, **106**, (2013), pp. 873–881. <https://doi.org/10.1016/j.compstruct.2013.07.002>.
- [11] M. Wang, Z. M. Li, and P. Qiao. Semi-analytical solutions to buckling and free vibration analysis of carbon nanotube-reinforced composite thin plates. *Composite Structures*, **144**, (2016), pp. 33–43. <https://doi.org/10.1016/j.compstruct.2016.02.025>.

- [12] Z. X. Lei, K. M. Liew, and J. L. Yu. Buckling analysis of functionally graded carbon nanotube-reinforced composite plates using the element-free kp-Ritz method. *Composite Structures*, **98**, (2013), pp. 160–168. <https://doi.org/10.1016/j.compstruct.2012.11.006>.
- [13] L. W. Zhang, Z. X. Lei, and K. M. Liew. Buckling analysis of FG-CNT reinforced composite thick skew plates using an element-free approach. *Composites Part B: Engineering*, **75**, (2015), pp. 36–46. <https://doi.org/10.1016/j.compositesb.2015.01.033>.
- [14] H. S. Shen and C. L. Zhang. Thermal buckling and postbuckling behavior of functionally graded carbon nanotube-reinforced composite plates. *Materials & Design*, **31**, (7), (2010), pp. 3403–3411. <https://doi.org/10.1016/j.matdes.2010.01.048>.
- [15] Y. Kiani. Thermal post-buckling of FG-CNT reinforced composite plates. *Composite Structures*, **159**, (2017), pp. 299–306. <https://doi.org/10.1016/j.compstruct.2016.09.084>.
- [16] H. V. Tung. Thermal buckling and postbuckling behavior of functionally graded carbon-nanotube-reinforced composite plates resting on elastic foundations with tangential-edge restraints. *Journal of Thermal Stresses*, **40**, (5), (2017), pp. 641–663. <https://doi.org/10.1080/01495739.2016.1254577>.
- [17] L. W. Zhang and K. M. Liew. Postbuckling analysis of axially compressed CNT reinforced functionally graded composite plates resting on Pasternak foundations using an element-free approach. *Composite Structures*, **138**, (2016), pp. 40–51. <https://doi.org/10.1016/j.compstruct.2015.11.031>.
- [18] M. Nasihatgozar, V. Daghigh, M. Eskandari, K. Nikbin, and A. Simoneau. Buckling analysis of piezoelectric cylindrical composite panels reinforced with carbon nanotubes. *International Journal of Mechanical Sciences*, **107**, (2016), pp. 69–79. <https://doi.org/10.1016/j.ijmecsci.2016.01.010>.
- [19] E. García-Macías, L. Rodríguez-Tembleque, R. Castro-Triguero, and A. Sáez. Buckling analysis of functionally graded carbon nanotube-reinforced curved panels under axial compression and shear. *Composites Part B: Engineering*, **108**, (2017), pp. 243–256. <https://doi.org/10.1016/j.compositesb.2016.10.002>.
- [20] H. S. Shen and Y. Xiang. Postbuckling of axially compressed nanotube-reinforced composite cylindrical panels resting on elastic foundations in thermal environments. *Composites Part B: Engineering*, **67**, (2014), pp. 50–61. <https://doi.org/10.1016/j.compositesb.2014.06.020>.
- [21] K. M. Liew, Z. X. Lei, J. L. Yu, and L. W. Zhang. Postbuckling of carbon nanotube-reinforced functionally graded cylindrical panels under axial compression using a meshless approach. *Computer Methods in Applied Mechanics and Engineering*, **268**, (2014), pp. 1–17. <https://doi.org/10.1016/j.cma.2013.09.001>.
- [22] H. S. Shen and Y. Xiang. Thermal postbuckling of nanotube-reinforced composite cylindrical panels resting on elastic foundations. *Composite Structures*, **123**, (2015), pp. 383–392. <https://doi.org/10.1016/j.compstruct.2014.12.059>.
- [23] H. S. Shen. Postbuckling of nanotube-reinforced composite cylindrical panels resting on elastic foundations subjected to lateral pressure in thermal environments. *Engineering Structures*, **122**, (2016), pp. 174–183. <https://doi.org/10.1016/j.engstruct.2016.05.004>.
- [24] L. T. N. Trang and H. V. Tung. Thermomechanical nonlinear analysis of axially compressed carbon nanotube-reinforced composite cylindrical panels resting on elastic foundations with tangentially restrained edges. *Journal of Thermal Stresses*, **41**, (4), (2018), pp. 418–438. <https://doi.org/10.1080/01495739.2017.1409093>.

- [25] H. V. Tung and L. T. N. Trang. Imperfection and tangential edge constraint sensitivities of thermomechanical nonlinear response of pressure-loaded carbon nanotube-reinforced composite cylindrical panels. *Acta Mechanica*, **229**, (5), (2018), pp. 1949–1969. <https://doi.org/10.1007/s00707-017-2093-z>.
- [26] H. S. Shen. Postbuckling of nanotube-reinforced composite cylindrical shells in thermal environments, Part I: Axially-loaded shells. *Composite Structures*, **93**, (8), (2011), pp. 2096–2108. <https://doi.org/10.1016/j.compstruct.2011.02.011>.
- [27] H. S. Shen. Postbuckling of nanotube-reinforced composite cylindrical shells in thermal environments, Part II: Pressure-loaded shells. *Composite Structures*, **93**, (10), (2011), pp. 2496–2503. <https://doi.org/10.1016/j.compstruct.2011.04.005>.
- [28] H. S. Shen and Y. Xiang. Postbuckling of nanotube-reinforced composite cylindrical shells under combined axial and radial mechanical loads in thermal environment. *Composites Part B: Engineering*, **52**, (2013), pp. 311–322. <https://doi.org/10.1016/j.compositesb.2013.04.034>.
- [29] H. S. Shen. Torsional postbuckling of nanotube-reinforced composite cylindrical shells in thermal environments. *Composite Structures*, **116**, (2014), pp. 477–488. <https://doi.org/10.1016/j.compstruct.2014.05.039>.
- [30] H. S. Shen. Thermal buckling and postbuckling behavior of functionally graded carbon nanotube-reinforced composite cylindrical shells. *Composites Part B: Engineering*, **43**, (3), (2012), pp. 1030–1038. <https://doi.org/10.1016/j.compositesb.2011.10.004>.
- [31] R. Ansari, T. Pourashraf, R. Gholami, and A. Shahabodini. Analytical solution for nonlinear postbuckling of functionally graded carbon nanotube-reinforced composite shells with piezoelectric layers. *Composites Part B: Engineering*, **90**, (2016), pp. 267–277. <https://doi.org/10.1016/j.compositesb.2015.12.012>.
- [32] D. G. Ninh. Nonlinear thermal torsional post-buckling of carbon nanotube-reinforced composite cylindrical shell with piezoelectric actuator layers surrounded by elastic medium. *Thin-Walled structures*, **123**, (2018), pp. 528–538. <https://doi.org/10.1016/j.tws.2017.11.027>.
- [33] J. E. Jam and Y. Kiani. Buckling of pressurized functionally graded carbon nanotube reinforced conical shells. *Composite Structures*, **125**, (2015), pp. 586–595. <https://doi.org/10.1016/j.compstruct.2015.02.052>.
- [34] M. Mirzaei and Y. Kiani. Thermal buckling of temperature dependent FG-CNT reinforced composite conical shells. *Aerospace Science and Technology*, **47**, (2015), pp. 42–53. <https://doi.org/10.1016/j.ast.2015.09.011>.
- [35] M. Mehri, H. Asadi, and Q. Wang. Buckling and vibration analysis of a pressurized CNT reinforced functionally graded truncated conical shell under an axial compression using HDQ method. *Computer Methods in Applied Mechanics and Engineering*, **303**, (2016), pp. 75–100. <https://doi.org/10.1016/j.cma.2016.01.017>.
- [36] R. Ansari and J. Torabi. Numerical study on the buckling and vibration of functionally graded carbon nanotube-reinforced composite conical shells under axial loading. *Composites Part B: Engineering*, **95**, (2016), pp. 196–208. <https://doi.org/10.1016/j.compositesb.2016.03.080>.
- [37] H. Huang and Q. Han. Nonlinear elastic buckling and postbuckling of axially compressed functionally graded cylindrical shells. *International Journal of Mechanical Sciences*, **51**, (7), (2009), pp. 500–507. <https://doi.org/10.1016/j.ijmecsci.2009.05.002>.
- [38] H. Huang and Q. Han. Nonlinear buckling and postbuckling of heated functionally graded cylindrical shells under combined axial compression and radial pressure. *International Journal of Non-Linear Mechanics*, **44**, (2), (2009), pp. 209–218. <https://doi.org/10.1016/j.ijnonlinmec.2008.11.016>.

- [39] H. V. Tung and P. T. Hieu. Nonlinear buckling of CNT-reinforced composite toroidal shell segment surrounded by an elastic medium and subjected to uniform external pressure. *Vietnam Journal of Mechanics*, **40**, (3), (2018), pp. 285–301. <https://doi.org/10.15625/0866-7136/12397>.
- [40] L. T. N. Trang and H. V. Tung. Buckling and postbuckling of carbon nanotube-reinforced composite cylindrical panels subjected to axial compression in thermal environments. *Vietnam Journal of Mechanics*, **40**, (1), (2018), pp. 47–61.

## APPENDIX A

The coefficients  $a_{j3}$  ( $j = 1 \div 4$ ) and  $a_{k4}$  ( $k = 1 \div 3$ ) in Eqs. (22b) and (22c) are

$$\begin{aligned}
 a_{13} &= a_{11}\beta_m^4 + a_{21}\delta_n^4 + a_{31}\beta_m^2\delta_n^2 + k_1 + k_2(\beta_m^2 + \delta_n^2) \\
 &\quad + \frac{\beta_m^2}{a_{12}\beta_m^4 + a_{22}\beta_m^2\delta_n^2 + a_{32}\delta_n^4} \left( \frac{\beta_m^2}{R} - a_{42}\beta_m^4 - a_{52}\beta_m^2\delta_n^2 - a_{62}\delta_n^4 \right) \left( \frac{1}{R} + a_{41}\delta_n^2 \right), \\
 a_{23} &= \frac{\beta_m^2\delta_n^2}{a_{12}\beta_m^4 + a_{22}\beta_m^2\delta_n^2 + a_{32}\delta_n^4} \left[ 2\frac{\beta_m^2}{R} + (a_{41} - a_{52})\beta_m^2\delta_n^2 - a_{42}\beta_m^4 - a_{62}\delta_n^4 \right] \\
 &\quad + \frac{\delta_n^2}{16a_{12}} \left( \frac{4}{R} - 16a_{42}\beta_m^2 \right), \\
 a_{33} &= \frac{\beta_m^4}{16a_{32}} + \frac{\delta_n^4}{16a_{12}}, \\
 a_{43} &= \frac{\beta_m^4\delta_n^4}{a_{12}\beta_m^4 + a_{22}\beta_m^2\delta_n^2 + a_{32}\delta_n^4} + \frac{\beta_m^4\delta_n^4}{81a_{12}\beta_m^4 + 9a_{22}\beta_m^2\delta_n^2 + a_{32}\delta_n^4}, \\
 a_{14} &= 4a_{11}\beta_m^4 + \frac{3}{4}k_1 + \beta_m^2k_2 - \frac{1}{4a_{12}R} \left( 4a_{42}\beta_m^2 - \frac{1}{R} \right), \\
 a_{24} &= \frac{\beta_m^2\delta_n^2}{2(a_{12}\beta_m^4 + a_{22}\beta_m^2\delta_n^2 + a_{32}\delta_n^4)} \left( \frac{\beta_m^2}{R} - a_{42}\beta_m^4 - a_{52}\beta_m^2\delta_n^2 - a_{62}\delta_n^4 \right) + \frac{\delta_n^2}{16a_{12}R}, \\
 a_{34} &= \frac{\beta_m^4\delta_n^4}{2(a_{12}\beta_m^4 + a_{22}\beta_m^2\delta_n^2 + a_{32}\delta_n^4)} + \frac{\beta_m^4\delta_n^4}{2(81a_{12}\beta_m^4 + 9a_{22}\beta_m^2\delta_n^2 + a_{32}\delta_n^4)}.
 \end{aligned} \tag{A1}$$

The details of coefficients  $f_{i1}$  ( $i = 1 \div 4$ ),  $f_{j2}$  ( $j = 1 \div 7$ ) and  $f_{k3}$  ( $k = 1 \div 7$ ) in the Eqs. (25)–(27) are defined as follows

$$\begin{aligned}
 f_{11} &= \frac{1}{2R_h^2} (1 - \nu_{12}\nu_{21}) \bar{e}_{21} + \frac{K_1 E_0^m}{2R_h^4}, \quad f_{21} = \frac{n^2}{8R_h^3} (1 - \nu_{12}\nu_{21}) \bar{e}_{21}, \\
 f_{31} &= \frac{\nu_{12}\bar{e}_{21}}{R_h\bar{e}_{11}}, \quad f_{41} = \frac{1}{R_h\bar{e}_{11}} (\bar{e}_{11}\bar{e}_{21T} - \nu_{12}\bar{e}_{21}\bar{e}_{11T}), \\
 f_{12} &= \bar{a}_{11} \frac{m^4\pi^4}{R_h^4L_R^4} + \bar{a}_{21} \frac{n^4}{R_h^4} + \bar{a}_{31} \frac{m^2n^2\pi^2}{R_h^4L_R^2} + K_1 \frac{E_0^m}{R_h^4} + K_2 \frac{E_0^m}{R_h^2} \left( \frac{m^2\pi^2}{R_h^2L_R^2} + \frac{n^2}{R_h^2} \right) \\
 &\quad + \left( \frac{m^2\pi^2}{R_h^3L_R^2} - \bar{a}_{42} \frac{m^4\pi^4}{R_h^4L_R^4} - \bar{a}_{52} \frac{m^2n^2\pi^2}{R_h^4L_R^2} - \bar{a}_{62} \frac{n^4}{R_h^4} \right) \left( \frac{\bar{a}_{41}m^2n^2\pi^2L_R^2 + m^2\pi^2R_hL_R^2}{\bar{a}_{12}m^4\pi^4 + \bar{a}_{22}m^2n^2\pi^2L_R^2 + \bar{a}_{32}n^4L_R^4} \right),
 \end{aligned}$$

$$\begin{aligned}
f_{22} &= \frac{n^2}{R_h^3} \bar{e}_{21} (1 - \nu_{12}\nu_{21}), \\
f_{32} &= \frac{1}{R_h^4 (\bar{a}_{12}m^4\pi^4 + \bar{a}_{22}m^2n^2\pi^2L_R^2 + \bar{a}_{32}n^4L_R^4)} \left[ \bar{a}_{41}m^4n^4\pi^4 + m^4n^2\pi^4R_h \right. \\
&\quad \left. + m^2n^2\pi^2R_h^4L_R^2 \left( \frac{m^2\pi^2}{R_h^3L_R^2} - \bar{a}_{42}\frac{m^4\pi^4}{R_h^4L_R^4} - \bar{a}_{52}\frac{m^2n^2\pi^2}{R_h^4L_R^2} - \bar{a}_{62}\frac{n^4}{R_h^4} \right) \right] \\
&\quad + \frac{n^2}{16\bar{a}_{12}R_h^2} \left( \frac{4}{R_h} - 16\bar{a}_{42}\frac{m^2\pi^2}{R_h^2L_R^2} \right) + \frac{n^2\bar{e}_{21}}{2R_h^3} (1 - \nu_{12}\nu_{21}), \\
f_{42} &= \frac{m^4\pi^4}{16\bar{a}_{32}R_h^4L_R^4} + \frac{n^4}{16\bar{a}_{12}R_h^4} + \frac{n^4\bar{e}_{21}}{8R_h^4} (1 - \nu_{12}\nu_{21}), \\
f_{52} &= \frac{m^4n^4\pi^4}{R_h^4 (\bar{a}_{12}m^4\pi^4 + \bar{a}_{22}m^2n^2\pi^2L_R^2 + \bar{a}_{32}n^4L_R^4)} \\
&\quad + \frac{m^4n^4\pi^4}{R_h^4 (81\bar{a}_{12}m^4\pi^4 + 9\bar{a}_{22}m^2n^2\pi^2L_R^2 + \bar{a}_{32}n^4L_R^4)}, \\
f_{62} &= \frac{m^2\pi^2}{R_h^2L_R^2} + \nu_{12}\frac{n^2\bar{e}_{21}}{R_h^2\bar{e}_{11}}, \quad f_{72} = \frac{n^2}{R_h^2\bar{e}_{11}} (\bar{e}_{11}\bar{e}_{21T} - \nu_{12}\bar{e}_{21}\bar{e}_{11T}), \\
f_{13} &= K_1\frac{E_0^m}{R_h^4} + \frac{\bar{e}_{21}}{R_h^2} (1 - \nu_{12}\nu_{21}), \\
f_{23} &= \frac{\bar{e}_{21}}{2R_h^2} (1 - \nu_{12}\nu_{21}) + 4\bar{a}_{11}\frac{m^4\pi^4}{R_h^4L_R^4} + K_1\frac{3E^m}{4R_h^4} + K_2\frac{m^2\pi^2E^m}{R_h^4L_R^2} - \frac{1}{4R_h\bar{a}_{12}} \left( 4\bar{a}_{42}\frac{m^2\pi^2}{R_h^2L_R^2} - \frac{1}{R_h} \right), \\
f_{33} &= \frac{n^2\bar{e}_{21}}{8R_h^3} (1 - \nu_{12}\nu_{21}) + \frac{n^2}{16\bar{a}_{12}R_h^3} \\
&\quad + \frac{m^2n^2\pi^2L_R^2}{2(\bar{a}_{12}m^4\pi^4 + \bar{a}_{22}m^2n^2\pi^2L_R^2 + \bar{a}_{32}n^4L_R^4)} \left( \frac{m^2\pi^2}{R_h^3L_R^2} - \bar{a}_{42}\frac{m^4\pi^4}{R_h^4L_R^4} - \bar{a}_{52}\frac{m^2n^2\pi^2}{R_h^4L_R^2} - \bar{a}_{62}\frac{n^4}{R_h^4} \right), \\
f_{43} &= \frac{m^4n^4\pi^4}{2R_h^4 (\bar{a}_{12}m^4\pi^4 + \bar{a}_{22}m^2n^2\pi^2L_R^2 + \bar{a}_{32}n^4L_R^4)} \\
&\quad + \frac{m^4n^4\pi^4}{2R_h^4 (81\bar{a}_{12}m^4\pi^4 + 9\bar{a}_{22}m^2n^2\pi^2L_R^2 + \bar{a}_{32}n^4L_R^4)}, \\
f_{53} &= \frac{m^2\pi^2}{R_h^2L_R^2}, \quad f_{63} = \frac{\nu_{12}\bar{e}_{21}}{R_h\bar{e}_{11}}, \quad f_{73} = \frac{1}{R_h\bar{e}_{11}} (\bar{e}_{11}\bar{e}_{21T} - \nu_{12}\bar{e}_{21}\bar{e}_{11T}).
\end{aligned} \tag{A2}$$

### APPENDIX B

The coefficients  $f_{i4}, f_{i5}$  ( $i = 1 \div 5$ ) in the Eqs. (29) are defined as

$$\begin{aligned} (f_{14}, f_{24}, f_{34}, f_{44}, f_{54}) &= \frac{1}{f_{64}} (f_{21}f_{32} - f_{11}f_{42}, -f_{21}f_{52}, f_{21}f_{62} - f_{31}f_{42}, f_{21}f_{72} - f_{41}f_{42}, f_{21}f_{12}), \\ (f_{15}, f_{25}, f_{35}, f_{45}, f_{55}) &= \frac{1}{f_{65}} (2f_{11}f_{32} - f_{11}f_{22}, -2f_{11}f_{52}, 2f_{11}f_{62} - f_{31}f_{22}, 2f_{11}f_{72} - f_{41}f_{22}, 2f_{11}f_{12}), \end{aligned} \quad (\text{B1})$$

in which

$$f_{64} = f_{65} = 2f_{11}f_{42} - f_{21}f_{22}, \quad (\text{B2})$$

The coefficients  $f_{j6}$  ( $j = 1 \div 8$ ) in the Eq. (30) are defined as

$$\begin{aligned} f_{16} &= f_{33}f_{35} - f_{13}f_{34} - f_{63}, & f_{26} &= f_{53} - f_{43}f_{35}, & f_{36} &= f_{33}f_{55} - f_{13}f_{54}, \\ f_{46} &= f_{13}f_{14} + f_{23} - f_{33}f_{15} - f_{43}f_{55}, & f_{56} &= f_{13}f_{24} - f_{33}f_{25} + f_{43}f_{15}, \\ f_{66} &= f_{43}f_{25}, & f_{76} &= f_{33}f_{45} - f_{13}f_{44} - f_{73}, & f_{86} &= -f_{43}f_{45}. \end{aligned} \quad (\text{B3})$$